Observation of line emissions from Ni-like W^{46+} ions in wavelength range of 7-8 Å in the Large Helical Device

Tetsutarou OISHI[1,2], Shigeru MORITA[1,2], Daiji KATO[1,3], Izumi MURAKAMI[1,2], Hiroyuki A. SAKAUE[1], Yasuko KAWAMOTO[1], Motoshi GOTO[1,2] and the LHD Experiment Group[1]

[1] *National Institute for Fusion Science, National Institutes of Natural Sciences, 322-6 Oroshi-cho, Toki 509-5292, Gifu, Japan*

[2] *Department of Fusion Science, The Graduate University for Advanced Studies, SOKENDAI, 322-6 Oroshi-cho, Toki 509-5292, Gifu, Japan*

[3] *Department of Advanced Energy Engineering Science, Kyushu University, Kasuga 816-8580, Fukuoka, Japan*

Abstract

Tungsten W^{46+} lines were successfully observed in the extreme ultraviolet (EUV) wavelength range of 7~8 Å in the Large Helical Device (LHD). Tungsten ions are distributed in the neutral beam injection (NBI) heated LHD plasma by injecting a pellet consisting of a small piece of tungsten metal wire enclosed by a carbon tube. While the electron temperature has a sudden drop due to the pellet injection, it can be recovered by electron cyclotron heating (ECH) superposition together with continuous NBI heating. It is found that a W^{46+} line at 7.92 Å is emitted when the central electron temperature ranges around 3.4 keV with relatively high intensity and is isolated from other intrinsic impurity lines. The 7.92 Å line consists of two lines of forbidden transitions which are blended with each other; an electric quadrupole (E2) transition at 7.928 Å and a magnetic octupole (M3) transition at 7.938 Å. The result is the first observation of W^{46+} lines for the stellarator experiments. The electron temperature dependence of the emission intensity of the 7.92 Å line agreed well with that of the fractional

abundance of W^{46+} ions calculated using the ionization and recombination rate coefficients registered in the ADAS database under the assumption of the collisional ionization equilibrium.

Keywords: plasma spectroscopy, extreme ultraviolet, magnetically confined fusion, impurity transport, highly ionized tungsten ions, forbidden transition

1. Introduction

Tungsten (W) is regarded as a possible candidate material for the plasma facing component (PFC) in divertor region of ITER and future fusion reactors because of its high melting point, low sputtering yield, and low tritium retention [1–3]. One of the major concerns is that the W ion causes a large energy loss by radiation and ionization due to its large atomic number of Z = 74 when the plasma is contaminated by the W impurity. Therefore, studies of W behaviors in high temperature plasmas are quite important for controlling W transport, which is necessary to establish a reliable operation scenario of fusion reactors. Figure 1 shows fractional abundance of W ions for each charge state calculated using the ionization and recombination rate coefficients registered in the ADAS database [4]. The definition of the fractional abundance, f_q, is the ratio of W ion density in a particular charge state q, n_q, to the total W ion density, $\Sigma_q n_q$, namely, $f_q = n_q / \Sigma_q n_q$ and $\Sigma_q f_q = 1$. f_q was calculated based upon an assumption of collisional ionization equilibrium where f_q is determined by a balance between ionization and recombination, such as $S_q f_q = \alpha_{q+1} n_{q+1}$, where S_q and α_{q+1} are the rate coefficients of ionization from q to $q+1$ and recombination from $q+1$ to q, respectively. Here we used the coefficients in the ADAS database of S_q calculated by Loch *et al* [5] (data type "*ADF11*", data file "*scd50_w.dat*") and α_q calculated by Post *et al* [6] followed by modification by Pütterich *et al* [7] (data type "*ADF11*", data file "*acd50_w.dat*"). As shown in Fig. 1, W^{46+} has the largest fractional abundance among all charge states in the T_e range of 3.5~6 keV. The maximum value is approximately 35 % at 4.4 keV. One of the reasons for the large fractional abundance of W^{46+} is a large difference of the ionization potential, E_i, between W^{45+} (E_i, = 2414 eV) and W^{46+} (E_i, = 4057 eV), because W^{46+} has a Ni-like, closed-shell electron configuration. Thus, we can expect that W^{46+} has a significant potential to be a good indicator of tungsten behaviors in a wide T_e range. However, only a few cases of observation of the W^{46+} line emissions have been reported in the fusion plasma experiments, such as a blended line of 3d-4s forbidden transitions of an electric quadrupole (E2) transition and a magnetic octupole (M3) transition observed in ASDEX-U tokamak at 7.93 Å [8], and a 3p-4d inner shell excitation line observed in JET tokamak at 5.20 Å [9]. Therefore, more integration of the spectroscopic data in the fusion plasma experiments is required to proceed with a comparison with the results of the electron beam ion trap (EBIT) experiments [10] and the atomic modelling calculations [11] in order to investigate characteristics of the W^{46+} line emissions more precisely.

Recently, several W^{46+} lines were successfully observed in the extreme ultraviolet (EUV) wavelength range of 7~8 Å in the Large Helical Device (LHD), which is a heliotron type plasma confinement device, as the first observation of W^{46+} lines for the stellarator experiments. In the present study, the EUV wavelength spectra and the temporal evolution and the electron temperature dependence of the intensities of the W^{46+} line will be investigated together with emission from tungsten ions in neighboring charge states such as W^{41+}~W^{45+} observed simultaneously in a single discharge to ensure the line identification.

2. Tungsten pellet injection experiment in LHD

LHD is a heliotron type plasma confinement device which has the major/minor radii of 3.6/0.64 m in the standard magnetic configuration with maximum plasma volume of 30 m^3 and toroidal magnetic field of 3 T [12]. The coil system consists of a set of two continuous superconducting helical coils with poloidal pitch number of 2 and toroidal pitch number of 10, and also three pairs of superconducting poloidal coils. Spectroscopic studies for emissions released from W ions in a combination with a W pellet injection technique have been intensively conducted in LHD for contribution to the W transport study in W-divertor fusion devices represented by ITER and for the expansion of the experimental database of W line emissions [13-16]. As the results of the previous studies, the line emissions from W ions in low charge states, W^{3+}~W^{6+}, have been identified in the vacuum ultraviolet (VUV) range of 500 - 1500Å [17]. Also in the EUV range of 10 - 500 Å, W ions in low charge states, W^{4+}~W^{7+}, medium charge states, W^{24+}~W^{33+} in the structures of the unresolved transition array (UTA), as well as high charge states, W^{41+}~W^{45+}, have been identified [18,19]. The line emissions from the neutral atoms, W^0, as well as the singly-ionized ions, W^+, were observed using a visible spectroscopy in the wavelength range of 4000 - 4400 Å [13]. The visible spectroscopy has also observed magnetic-dipole (M1) transition lines from W^{26+} and W^{27+} in the wavelength range of 3300 - 3900 Å [20,21]. In the studies introduced above, W ions were distributed in the NBI-heated LHD plasma by injecting a pellet consisting of a small piece of W metal wire enclosed by a carbon or polyethylene pellet with the shape of a cylindrical tube [15]. Figure 2 illustrates a schematic drawing of the spectroscopy system using flat-field grazing incidence EUV spectrometers which are denoted as "EUV Short" and "EUV Long" covering the wavelength range of 5-130 Å and 50-500 Å, respectively [22,23]. Top view of magnetic surfaces with the position of the magnetic axis, R_{ax}, of 3.6 m, optical axis of two spectrometers, incident direction of impurity pellet, and a plasma cross section including optical axis of the EUV spectrometers are shown together.

Figure 3 shows a typical waveform of the W pellet injection experiment in a hydrogen discharge with R_{ax}, of 3.6 m at toroidal magnetic field, B_t, of 2.75 T in the counter-clockwise direction. In this discharge, the length and the diameter of a W wire enclosed in a carbon pellet were 0.7 mm and 0.1 mm, respectively. Then, the number of atoms enclosed in a pellet, N_W, was 3.5×10^{17}. As shown in Fig. 3(a), the plasma was initiated by the electron cyclotron heating (ECH), and further heated by the neutral hydrogen beams. Figures 3 (b), (c), (d) and (e) show the central electron temperature, T_{e0}, the line-averaged electron density, n_e, the plasma stored energy, W_p, and the total radiation power, P_{rad}, respectively. After the tungsten pellet injection at 4.1 s, T_{e0} and W_p quickly decreased, while n_e increased. In our previous experiments, T_{e0} continued decreasing after the pellet injection and was sustained in a steady state with $T_{e0} < 1$ keV [16]. On the other hand, ECH was superposed after the pellet injection in the present study to recover T_{e0} to observe the highly-ionized W ions. As a result of the ECH superposition for 4.2~4.7 s with the injection power of 3 MW, T_{e0} recovered up to approximately 3.4 keV. It is also worth noting that P_{rad} continued increasing during the ECH superposition phase up to the maximum value of ~5.3 MW at 5.0 s, which is one of the signs indicating that W ions were substantially accumulated within a confinement region with releasing emissions.

3. EUV spectra of W^{46+} in the wavelength range of 7-8 Å

Figure 4 (a) shows EUV spectrum including line emissions released from tungsten ions in the wavelength range of 5-60 Å measured using "EUV Short" spectrometer. The spectral data were averaged over 3.7~4.0 s, which corresponds to the temporal period before the pellet injection, and 4.2~4.5 s, which corresponds to the temporal period with the ECH superposition after the pellet injection. In this wavelength range, the unresolved transition arrays (UTAs) consisting of the line emissions from W^{23+}~W^{33+} and W^{24+}~W^{29+} ions were observed at 19 ~ 33 Å and 47 ~ 54 Å, respectively. These UTA spectra are clear signals indicating that the W ions are successfully distributed in the plasmas by the pellet injection, which have been observed in many fusion plasma experiments related to W impurity studies [13,14]. The wavelength range of 6.5 ~ 10 Å of the spectra in Fig. 4 (a) is enlarged and shown in Fig. 4 (b). Four peaks of W^{46+} line emissions were observed after the pellet injection. Even though most of the lines have weak intensities and are blended with UTA in 7.0 ~ 7.8 Å, it is found that a line at 7.92 Å is emitted with relatively high intensity and isolated from other lines. Table 1 summarizes the wavelength list of EUV lines from W^{46+} observed in this study. The first and the second columns give the wavelengths of line emissions from the NIST database [24], λ_{NIST}, and the present observation, λ_{obs}, respectively. Discrepancy between λ_{NIST} and λ_{obs} is shown in the third column. The lower and the upper level configurations are stated in the fourth and fifth columns, respectively. The sixth column gives the transition types for forbidden lines. Remarks on the observation are stated in the seventh column. λ_{obs} values of the lines blended with UTA in 7.0 ~ 7.8 Å are enclosed in parentheses. The 7.92 Å line observed in this study is considered to consist of two lines of forbidden transitions which are blended with each other; an E2 transition at 7.928 Å and an M3 transition at 7.938 Å.

Figure 5 illustrates a partial energy level diagram of transitions in $3d^{10}$ ground and $3d^94s$ and $3d^94p$ excited configurations of a Ni-like W^{46+} ion [24]. Ni-like ions have a closed shell structure with the $3d^{10}$ electron configuration as the ground state, thus, transitions from the first excited state of $3d^94s$ to the ground state are forbidden transitions. Italic fonts indicate wavelengths of the E2 and the M3 forbidden transitions observed in this work.

In order to ensure the correctness of the line identification, temporal behaviors of the line intensities of the newly observed W^{46+} line is compared to those of well-known W lines in neighboring charge states. Figures 6 and 7 show temporal evolution of EUV spectra in the wavelength range of 6.5-10 Å measured using "EUV Short" spectrometer and 120-140 Å measured using "EUV Long" spectrometer, respectively, before and after the W pellet injection. No W emission lines were found in the time ranges of 4.0~4.1 s before the W pellet injection as shown in Figs. 6(a) and 7(a) as well as 4.1~4.2 s just after the W pellet injection as shown in Figs. 6(b) and 7(b). When ECH was superposed at 4.2 s, T_{e0} recovered and reached up to 3.4 keV accompanied by spectral peaks of W^{44+}~W^{46+} as shown in Figs. 6(c,d) and W^{41+}~W^{45+} as shown in Figs. 7(c,d). Then the line intensities of the peaks turned to decrease with T_{e0} as shown in Figs. 6(e-h) and in Figs. 7(e-h). Figure 8 shows temporal evolutions of (a) T_{e0} and central electron density, n_{e0}, line intensities of (b) W^{46+} 7.92 Å measured using "EUV Short" spectrometer, (c) W^{45+} 127.00 Å, (d) W^{43+} 126.29 Å, (e) W^{42+} 129.41 Å, and (f) W^{41+} 131.21 Å measured using "EUV Long" spectrometer. The line intensity was evaluated by integrating in the wavelength range of 7.89~7.95 Å for W^{46+} 7.92 Å, 126.93~127.25 Å for W^{45+} 127.00 Å, 126.13~126.45 Å for W^{43+} 126.29 Å, 129.19~129.51 Å for W^{42+} 129.41 Å, and 130.97~131.30 Å for W^{41+} 131.21 Å. The signal levels in neighboring wavelength ranges which have no significant line emissions were subtracted from the W line intensities as background levels mainly consisting of bremsstrahlung emissions. As shown in the figures, line emissions from

W ions in the higher charge states such as W^{46+} and W^{45+} had large intensities just after the onset of ECH superposition of 4.2 s with T_{e0} ~ 3.4 keV while the lower charge states such as W^{42+} and W^{41+} became dominant as T_{e0} decreased down to 2.6 keV around t = 4.6 s. Considering E_i, for each charge state analyzed in this study, 1995 eV, 2149 eV, 2210 eV, 2414 eV, and 4057 eV for W^{41+}, W^{42+}, W^{43+}, W^{45+}, and W^{46+}, respectively, this sequential behavior for each charge state is reasonable for the relationship between the electron temperature and the ionization potential.

Figure 9 shows the line intensity of (a) W^{46+} 7.92 Å, (b) W^{45+} 127.00 Å, (c) W^{43+} 126.29 Å, (d) W^{42+} 129.41 Å, and (e) W^{41+} 131.21 Å normalized to n_{e0} as a function of T_{e0} together with the fractional abundance which has been already shown in Fig. 1. The T_{e0} dependence of both the emission intensity and the fractional abundance are almost identical for each charge state. The result indicates that the line identification for the W^{46+} line is adequate and dependence of the line intensity on T_{e0} can be explained by the assumption of the collisional ionization equilibrium.

Finally, observability of W^{46+} lines is discussed as diagnostics tools for tungsten behaviors in the metal-wall devices. According to the NIST database, there are several lines of which the wavelengths are close to W^{46+} 7.928 Å and 7.938 Å. Figure 10 shows ionization potentials of typical metal impurity ions which release line emissions with wavelengths close to W^{46+} 7.928 Å and 7.938 Å. The ionization potential of W^{46+} is isolated from that of other lines as shown in Fig. 10. Therefore, line-blending with the other lines may not be so serious in the experimental conditions which are suitable for observation of the W^{46+} lines.

4. Summary

Tungsten W^{46+} lines were successfully observed in the EUV wavelength range of 7~8 Å in the W pellet injection experiment in LHD. While T_{e0} has a sudden drop due to the pellet injection, T_{e0} is recovered by ECH superposition together with continuous NBI heating. It is found that

W^{46+} line at 7.92 Å is emitted when the central electron temperature ranges around 3.4 keV with relatively high intensity and is isolated from other intrinsic impurity lines. The 7.92 Å line is considered to consist of two lines of forbidden transitions which are blended with each other; an E2 transition at 7.928 Å and an M3 transition at 7.938 Å. The result is the first observation of W^{46+} line for the stellarator experiments. The 7.92 Å line will be a useful tool for the measurements of spatial profile and temporal evolution of W^{46+} ions for future studies.

Acknowledgments

The authors thank all the members of the LHD team for their cooperation with the LHD operation. This work is partially supported by the LHD project financial support (ULPP010, ULPP038) and Grant-in-Aid for Young Scientists (B) (17K14426).

References

[1] ITER Physics Basis Editors, ITER Physics Expert Group Chairs and Co-Chairs and ITER Joint Central Team and Physics Integration Unit, Nucl. Fusion **39** (1999) 2137.

[2] R. Neu, R. Dux, A. Kallenbach et al., Nucl. Fusion **45** (2005) 209.

[3] J. Roth, E. Tsitrone, T. Loarer et al., Plasma Phys. Control. Fusion **50** (2008) 103001.

[4] OPEN-ADAS Project 1995–2020 http://open.adas.ac.uk

[5] S. D. Loch, J. A. Ludlow, M. S. Pindzola et al., Phys. Rev. A **72** (2005) 052716.

[6] D.E. Post, R. Jensen, C. Tarter *et al.,* At. Data Nucl. Data Tables **20** (1977) 397.

[7] T. Pütterich, R. Neu, R. Dux *et al.*, Plasma Phys. Control. Fusion **50** (2008) 085016.

[8] R. Neu, K. B. Fournier, D Schögl et al., J. Phys. B: At. Mol. Opt. Phys. **30** (1997) 5057.

[9] T. Nakano, A. E. Shumack, C. F. Maggi et al., J. Phys. B: At. Mol. Opt. Phys. **48** (2015) 144023.

[10] J. Clementson, P. Beiersdorfer, and M. F. Gu, Phys. Rev. A **81** (2010) 012505.

[11] Y. Ralchenko, J. Phys. B: At. Mol. Opt. Phys. **40** (2007) F175.

[12] Y. Takeiri, T. Morisaki, M. Osakabe et al., Nucl. Fusion **57** (2017) 102023.

[13] S. Morita, C. F. Dong, M. Goto et al., AIP Conf. Proc. **1545** (2013) 143.

[14] S. Morita, C. F. Dong, D. Kato et al., Journal of Physics: Conf. Series **1289** (2019) 012005.

[15] X. L. Huang, S. Morita, T. Oishi et al., Rev. Sci. Instrum. **85** (2014) 11E818.

[16] T. Oishi, S. Morita, X. L. Huang et al., Plasma Fusion Res. **13** (2018) 3402031

[17] T. Oishi, S. Morita, X. L. Huang et al., Phys. Scr. **91** (2016) 025602

[18] Y. Liu, S. Morita, T. Oishi et al., Plasma Fusion Res. **13** (2018) 3402020

[19] Y. Liu, S. Morita, T. Oishi et al., J. Appl. Phys. **122** (2017) 233301

[20] D. Kato, M. Goto, S Morita et al., Phys. Scr. **T156** (2013) 014081

[21] D. Kato, H. A. Sakaue, I. Murakami et al., Proc. 26th IAEA Fusion Energy Conf. (2016, Kyoto) EX/P8-14

[22] M. B. Chowdhuri, S. Morita, M. Goto et al., Appl. Opt. **47** (2008) 135.

[23] M. B. Chowdhuri, S. Morita, M. Goto et al., Rev. Sci. Instrum. **78** (2007) 023501.

[24] A. Kramida *et al.*, (2019). NIST Atomic Spectra Database (ver. 5.7.1), [Online]. Available: https://physics.nist.gov/asd [2020, July 19]. National Institute of Standards and Technology, Gaithersburg, MD.

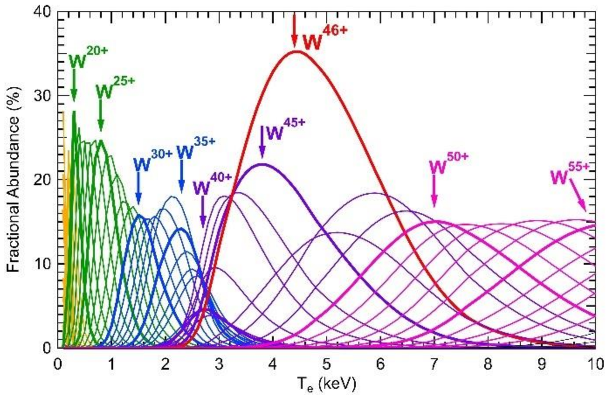

Figure 1 Fractional abundance of tungsten ions in each charge state calculated using the ionization and the recombination rate coefficients registered in the ADAS database.

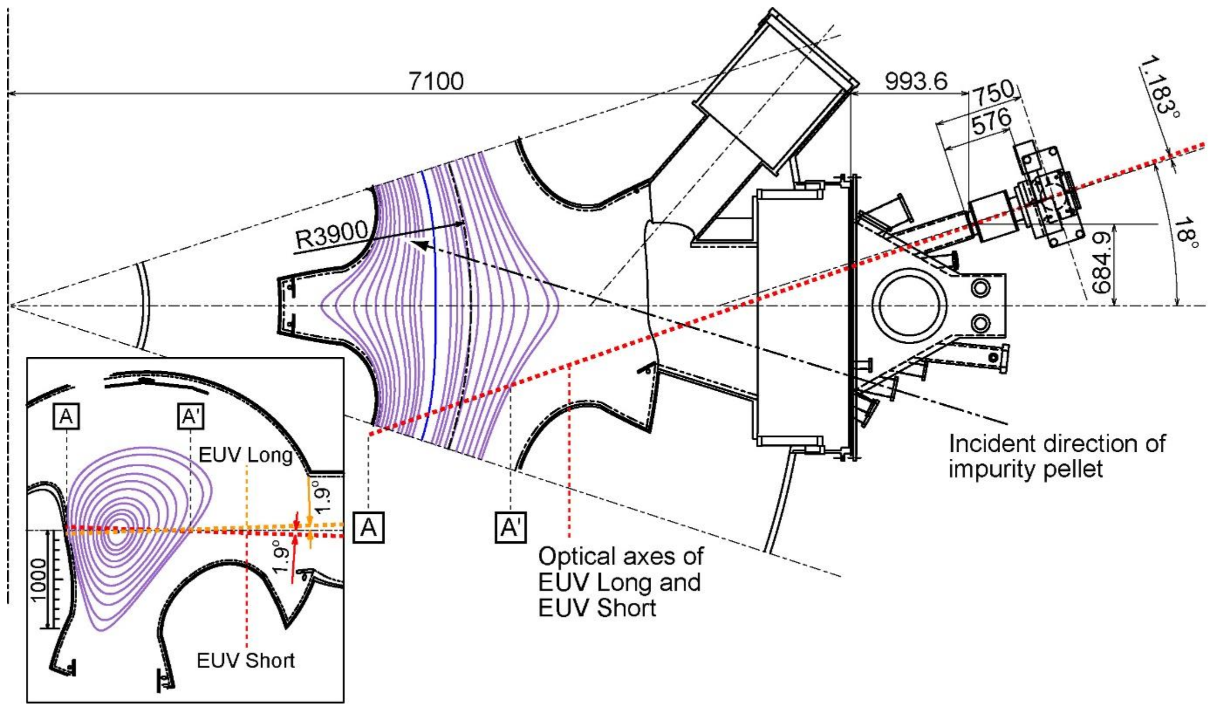

Figure 2 Schematic drawing of EUV spectroscopy system using flat-field grazing incidence EUV spectrometers in LHD. Top view of magnetic surfaces (R_{ax} = 3.6m), optical axes of two spectrometers ("EUV Long" and "EUV Short"), incident direction of impurity pellet, and a plasma cross section including optical axes of two spectrometers shown together.

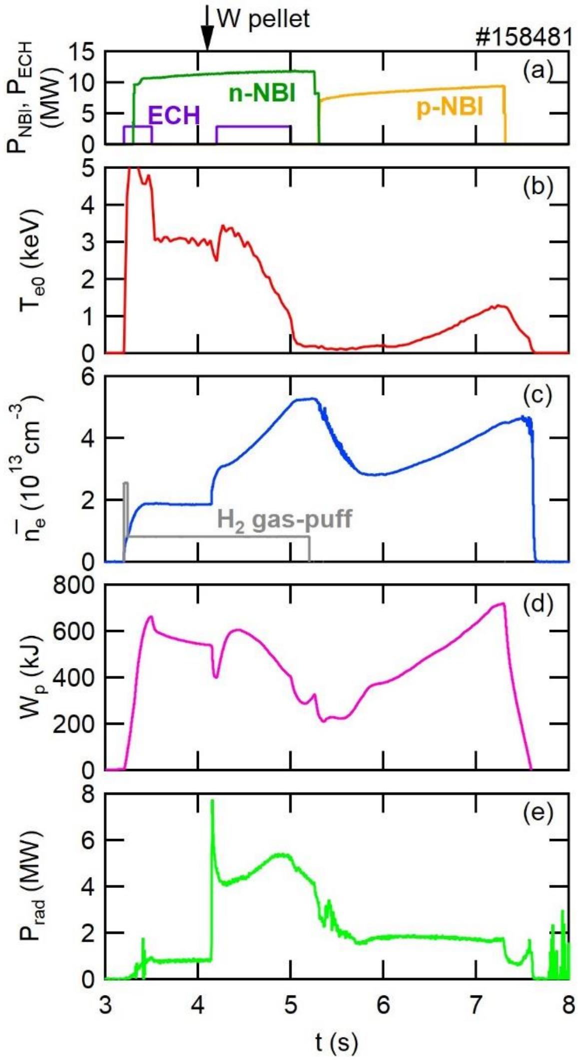

Figure 3 Typical waveform of W pellet injection experiment in LHD: (a) heating power of ECH, n-NBI, and p-NBI, (b) central electron temperature, (c) line-averaged electron density, (d) plasma stored energy, and (e) total radiation power.

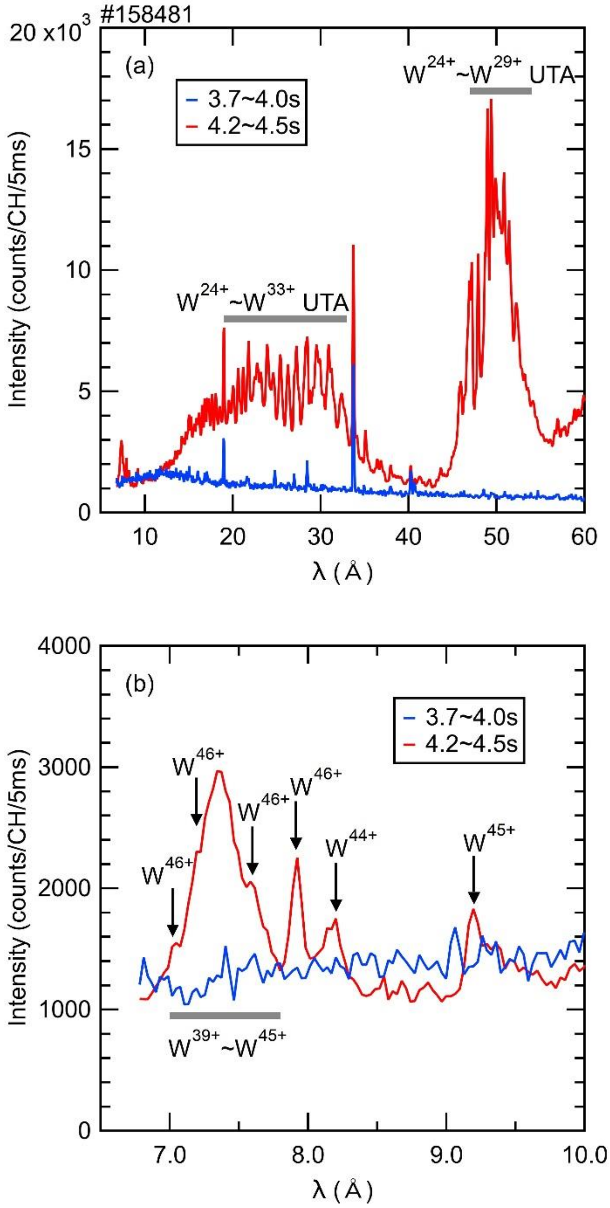

Figure 4 (a) Typical EUV spectrum including line emissions released from tungsten ions in the wavelength range of 5-60 Å. (b) An enlarged spectrum in the wavelength range of 6.5-10 Å. The spectral data were averaged over 3.7~4.0 s (before the pellet injection) and 4.2~4.5 s (with the ECH superposition after the pellet injection).

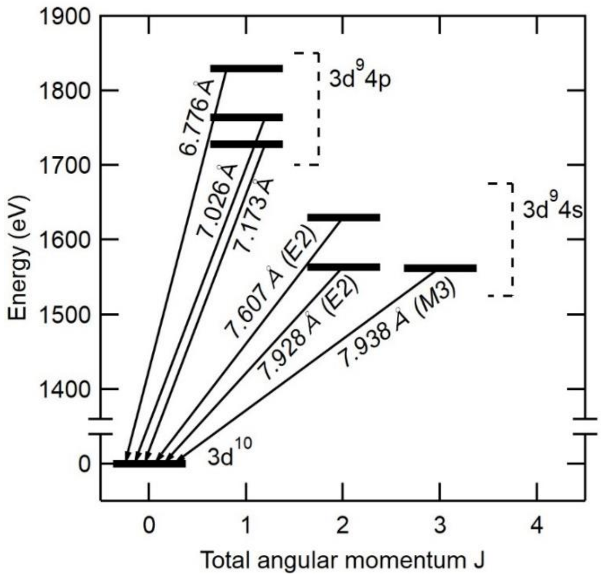

Figure 5 Partial energy level diagram of transitions in $3d^{10}$ ground and $3d^94s$ and $3d^94p$ excited configurations of Ni-like tungsten. Italic fonts indicate wavelengths of E2 and M3 transitions observed in this work.

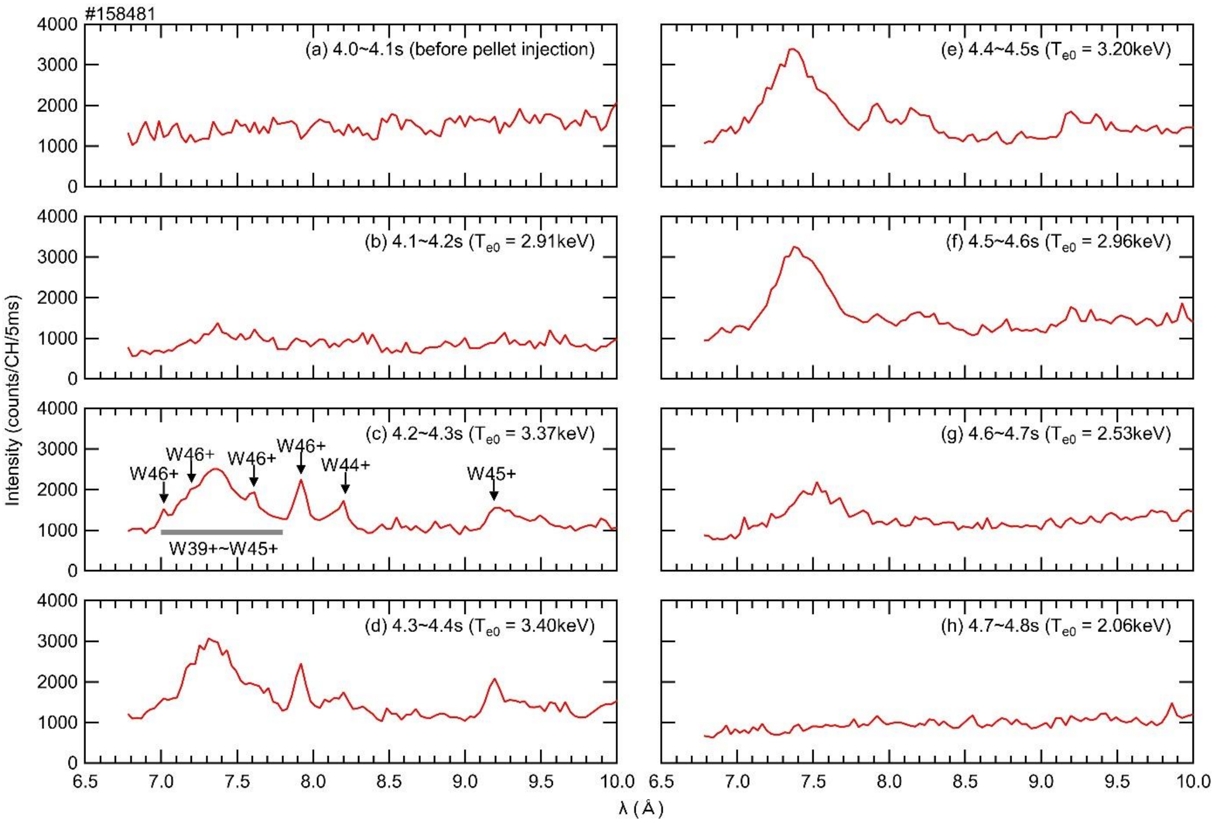

Figure 6 Temporal evolution of EUV spectrum in the wavelength range of 6.5-10 Å before and after the tungsten pellet injection.

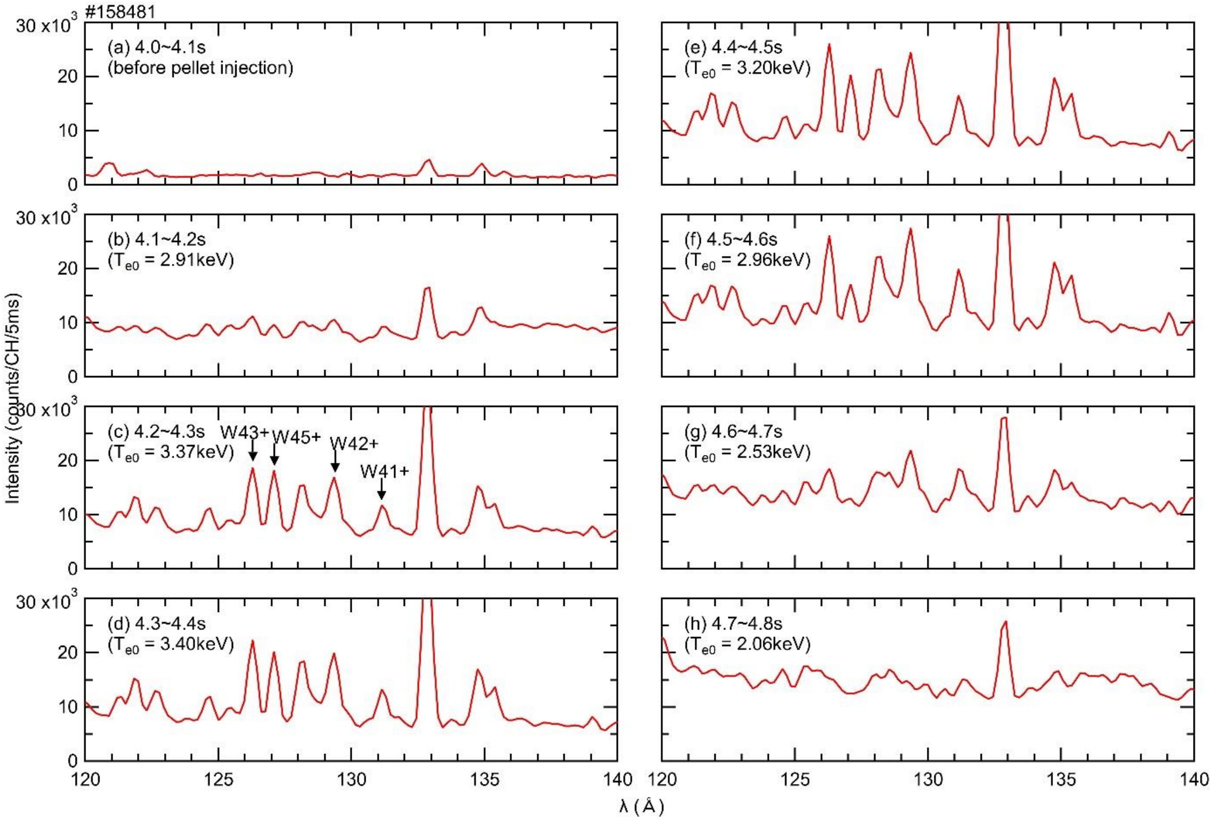

Figure 7 Temporal evolution of EUV spectrum in the wavelength range of 120-140 Å before and after the tungsten pellet injection.

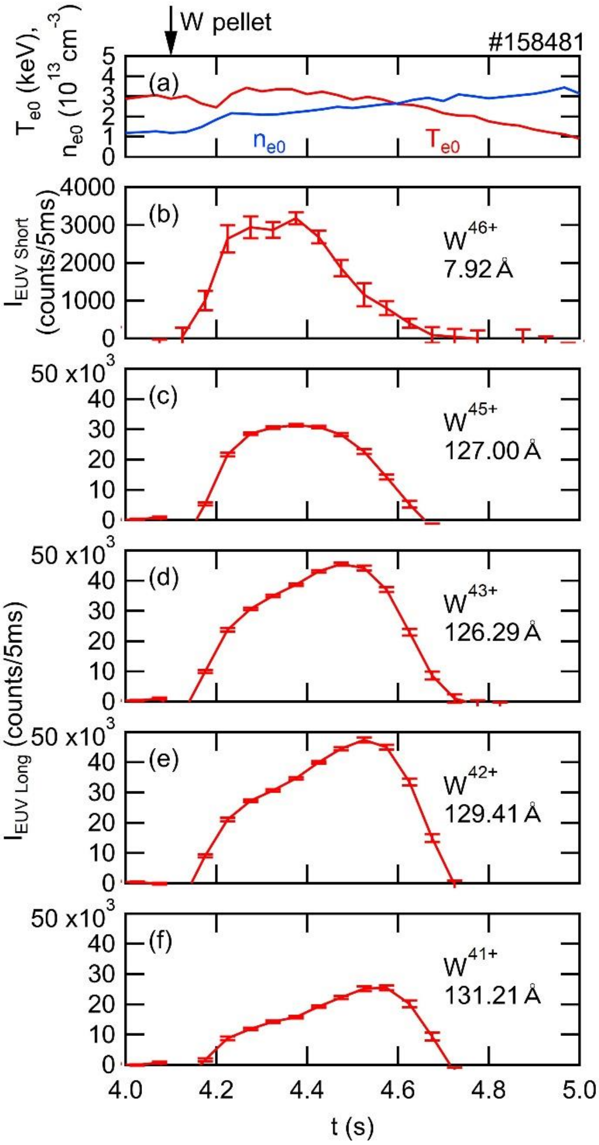

Figure 8 Temporal evolutions of (a) central electron temperature, T_{e0}, and density, n_{e0}, (b) line intensity of tungsten W^{46+} 7.92 Å measured using "EUV Short" spectrometer, (c-f) line intensities of W^{45+} 127.00 Å, W^{43+} 126.29 Å, W^{42+} 129.41 Å, and W^{41+} 131.21 Å measured using "EUV Long" spectrometer. ECH is superposed from 4.2 s to 5.0 s.

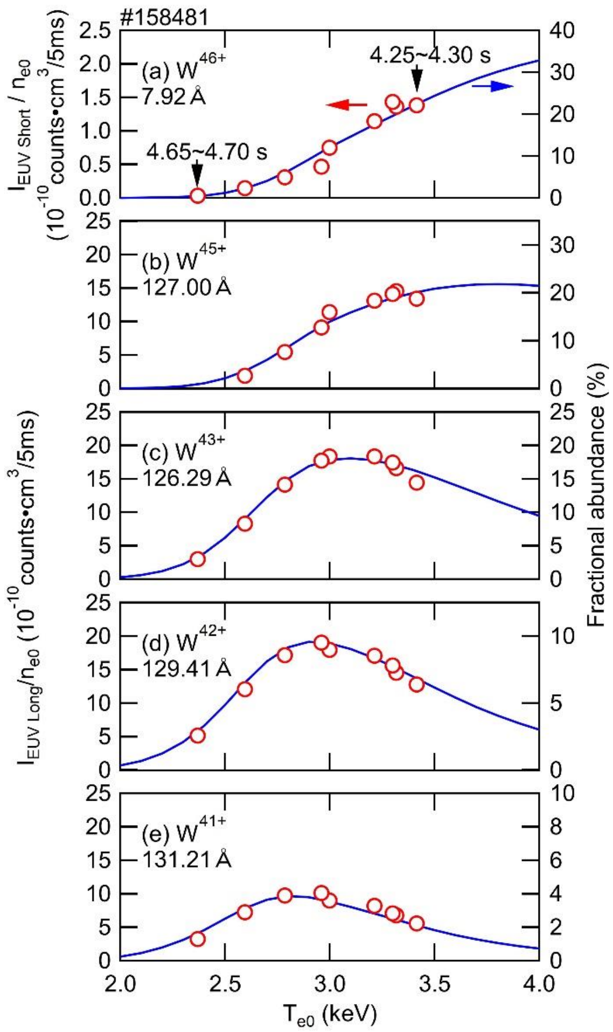

Figure 9 Line intensity of tungsten (a) W^{46+} 7.92 Å, (b) W^{45+} 127.00 Å, (c) W^{43+} 126.29 Å, (d) W^{42+} 129.41 Å, and (e) W^{41+} 131.21 Å as a function of central electron temperature, T_{e0}. The intensity is normalized to central electron density, n_{e0}. Blue solid lines are fractional abundance for each charge state calculated using the ionization and the recombination rate coefficients registered in the ADAS database.

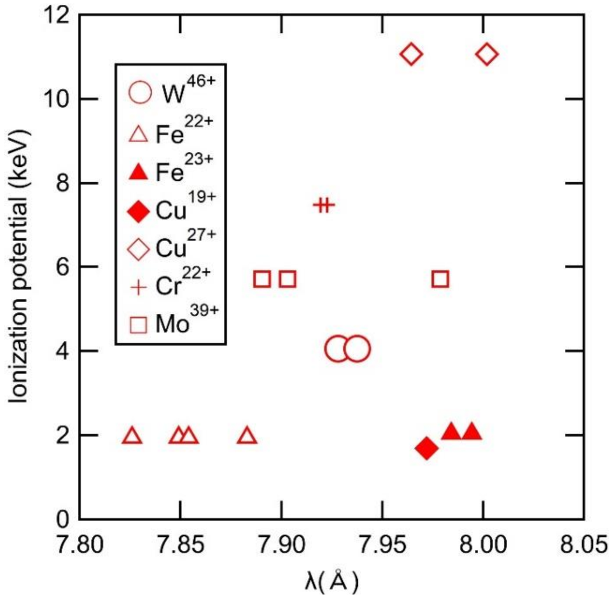

Figure 10 Ionization potentials of typical metal impurity ions which release line emissions with wavelengths close to W^{46+} 7.928 Å and 7.938 Å.

Table 1 Wavelength list of EUV lines from W^{46+} observed in this study. The first and the second columns give the wavelengths of line emissions from the NIST database, λ_{NIST}, and the present observation, λ_{obs}, respectively. Discrepancy between λ_{NIST} and λ_{obs} is shown in the third column. The lower and the upper level configurations are stated in the fourth and the fifth columns, respectively. The sixth column gives the transition types for forbidden lines. Remarks on the observation are stated in the seventh column. λ_{obs} values of the lines blended with UTA in 7.0 ~ 7.8 Å are enclosed in parentheses.

<table>
<tr><th>λ_{NIST} (Å)</th><th>λ_{obs} (Å)</th><th>$\lambda_{NIST} - \lambda_{obs}$ (Å)</th><th>Lower level configuration</th><th>Upper level configuration</th><th>Type</th><th>Remarks</th></tr>
<tr><td>7.026</td><td>(7.049 ± 0.008)</td><td>-0.023</td><td>$3p^63d^{10}$</td><td>$3p^63d^94p$</td><td></td><td rowspan="3">Blended with UTA in 7.0~7.8 Å</td></tr>
<tr><td>7.173</td><td>(7.212 ± 0.010)</td><td>-0.039</td><td>$3p^63d^{10}$</td><td>$3p^63d^94p$</td><td></td></tr>
<tr><td>7.607</td><td>(7.582 ± 0.003)</td><td>0.025</td><td>$3p^63d^{10}$</td><td>$3p^63d^94s$</td><td>E2</td></tr>
<tr><td>7.928</td><td rowspan="2">7.917 ± 0.001</td><td rowspan="2">-</td><td>$3p^63d^{10}$</td><td>$3p^63d^94s$</td><td>E2</td><td rowspan="2">Blended with each other</td></tr>
<tr><td>7.938</td><td>$3p^63d^{10}$</td><td>$3p^63d^94s$</td><td>M3</td></tr>
</table>